land

MDPI

Assessment and Forecast of Shoreline Change Using Geo-Spatial Techniques in the Gulf of California

Yedid Guadalupe Zambrano-Medina [1], Wenseslao Plata-Rocha [1], Sergio Alberto Monjardin-Armenta [1] and Cuauhtémoc Franco-Ochoa [2,*]

1   Facultad de Ciencias de la Tierra y el Espacio, Universidad Autónoma de Sinaloa, Culiacán 80013, Mexico
2   Facultad de Ingeniería Civil, Universidad Autónoma de Sinaloa, Culiacán 80013, Mexico
*   Correspondence: cfrancoo@uas.edu.mx; Tel.: +52-667-1567686

Abstract: In coastal regions, the combined effects of natural processes, human activity, and climate change have caused shoreline changes that may increase in the future. The assessment of these changes is essential for forecasting their future position for proper management. In this context, shoreline changes in the Gulf of California (GC), Mexico, have received little attention and no previous studies have addressed future forecasting. In this study, the researchers assessed the historical shoreline changes to forecast the long-term shoreline positions. To address this, shoreline data were obtained from Landsat satellite images for the years 1981, 1993, 2004, 2010, and 2020. The Net Shoreline Movement (NSM), Linear Regression Rate (LRR), End Point Rate (EPR), and Weighted Linear Regression (WLR) geo-spatial techniques were applied to estimate the shoreline change rate by using a Digital Shoreline Analysis System (DSAS) in the GIS environment. A Kalman filter model was used to forecast the position of the shoreline for the years 2030 and 2050. The results show that approximately 72% of the GC shoreline is undergoing steady erosion, and this trend is continuing in the future. This study has provided valuable and comprehensive baseline information on the state of the shoreline in the GC that can guide coastal engineers, coastal managers, and policymakers in Mexico to manage the risk. It also provides both long-term and large-scale continuous datasets that are essential for future studies focused on improving the shoreline forecast models.

Keywords: shoreline changes; coastal erosion; remote sensing; forecast; Gulf of California

1. Introduction

Shoreline analysis is essential for coastal zone monitoring and environmental protection, as well as for sustainable development. This is an ecological environmental zone of relative fragility and with ecosystems of great importance (for its high productivity and rich diversity) [1]. Currently, about 2.5 billion people (40% of the world population) live within 100 km of a coast, adding a further threat to coastal ecosystems [2]. In Mexico, approximately a quarter of the population lives on coastal plains. However, the rapid expansion of economic activities has caused a chaotic growth in coastal and city regions as well, as environmental struggles that have affected the shorelines [3].

The world's coasts, as well as that of GC, are governed by both anthropogenic and natural factors [4]. These processes have been present since the second half of the 20th century, generating critical erosion and accretion points. Intense anthropogenic effects have caused significant changes in the sediment and runoff, altering coastal systems and setting off coastal erosion of the largest deltas in the world [5]. Factors such as dams, irrigation, and land use practices have reduced the number of river sediments reaching the coast. Over the last 50 years, the construction of dams has become the predominant factor in the reduction in sediment reaching the coasts of the world [6].

Another major impact on coastal areas is the sea level rise. This mainly affects low-lying coastal areas because of the intensification of flooding, coastal erosion, and saltwater

intrusion in estuaries and coastal aquifers. In addition, the number of people affected are expected to increase by the end of this century [7]. According to data from the AVISO+ Satellite Altimetry Data, the global mean sea level increased at a rate of 3.41 mm/year in March 2020 compared to the rate of 3.37 mm/year recorded in 2015. It is predicted that an increase in the rate of the sea level rise will cause a worsening of the existing coastal erosion problem [8].

Mapping out, forecasting, and keeping tabs on shorelines are imperative for the administration of their natural resources. Support with environmental studies, sustainable development, coastal environmental protection, and planning are needed [9,10]. This study of the shoreline variation plays an important role in coastal zone management and becomes crucial in the context of climate change and sea level rise [11]. The monitoring of shoreline changes over time is essential for anticipating future coastal alterations, useful for recognizing coastal ecosystems, and provides vital data for understanding the coastal reactions to environmental fluctuations, climate change, and human-caused actions [12].

Two of the most important concepts for the monitoring of the coastal zones are Coastline [13], which is used to describe the boundary between the land and water at large regional scales, is unlike Shoreline, which refers to the intersection of water and land surfaces at a specific time [14]. That geographical line/object between the sea and the land at an instant in time [12], is used in this research.

The shoreline is considered unique in that it is one of the most dynamic and temporary geographic features in response to one or more factors, such as geology, geomorphology, wave action, periodic storms, sea level rise, sediment transport, and anthropogenic actions [15–17]. Causing the shoreline to constantly change results in (1) erosion, or (2) accretion [18]. The first describes the land being eroded because of a sediment reduction, while the second denotes land being built up because of sediment accumulation [19].

The coastal maps were created through the process of land surveying from 1807 to 1927, and the potential of aerial photographs to supplement coastal mapping from 1927 to 1980 was understood, being the only source available to produce such maps [20]. Estimates of the coast change can now be very accurate using field surveys, high-resolution aerial photography, periodic overflights, light detection and ranging (LiDAR) technology, synthetic aperture radar (SAR) imagery, and video skills. However, these techniques continue to be time-consuming, costly, and labor-intensive [21]. Currently, there are also free satellite images that offer higher temporal frequency, resolution, and global coverage, such as Landsat images, which have contributed significantly to the understanding of the environment [22]. In this way, remote sensing plays an important role in monitoring coastal zones, as shoreline variations have a direct impact on the economic development and land management [23,24].

Recently, indicators have emerged from satellite image processing techniques to extract a proxy of the shoreline that does not perforce to be visible to the human eye, as the absorption of the infrared wavelength of water and its strong reflectance by vegetation and soil make these images an ideal combination for mapping the spatial distribution of land and water [25–27]. On a global scale, the analysis of the spatiotemporal variations of the shoreline in research is addressed, e.g., [4,9,10,12,15–17]. Most coastal researchers use geospatial techniques as a method for shoreline determination and analysis, relying primarily on satellite imagery.

Among the most widely used methodologies by coastal researchers and national government institutions, has been the Digital Shoreline Analysis System (DSAS) to support unstable coastal decision-making and development activities [28]. Meanwhile, to represent a rate of change, the two most-used methods in research are EPR [4,29], because of its simplicity with obtaining results with only two shorelines, and LRR. The LRR method is more complete because it considers all shorelines in the observed time [19] and it is therefore more accepted as it is based on more rigorous statistics.

There is a variety of research on the exchange rate analysis on the coast. For example, [30] this method was used in Kenitra, the Moroccan Atlantic coast that is 10 km long,

for a period of 78 years (1936–2014), obtaining the shoreline from different data sources (topographic maps, aerial photographs, and field measurements). Daud, S. et al. [14] analyzed the trend of the shoreline change in Selangor of approximately 213 km with the support of Landsat satellite imagery for the years 1990–2015. Masria, A. et al. [23] applied the DSAS methodology, using Landsat images to obtain the shoreline for the years 1984–2004 northwest of the Nile delta on the Rosetta promontory coast of approximately 44 km. Dewidar, K. et al. [31] also applied the same methodology by obtaining the shoreline using Landsat imagery from 1972 to 2018 to monitor the fluctuation of erosion and accretion over 280 km of the Nile Delta shoreline. Yan, D. et al. [10] analyzed the temporal and spatial variation in the 530-km-long shoreline from 1983 to 2020 taken from Landsat imagery for the Yancheng shoreline using DSAS and forecasted the position of the shoreline for the years 2019 and 2020 based on the 1983–2009 and 1983–2010 position, respectively. However, despite the number of investigations using DSAS and satellite imagery, there have been few studies that address it for long stretches and that also forecast the future position of the shoreline.

The objectives of this study were to assess the shoreline changes between 1981 and 2020, and to forecast the shoreline position for the years 2030 and 2050. For evaluation, the assessment of the shoreline changes was based on a range of time scales using the shoreline extracted from Landsat satellite images of the years 1981, 1993, 2004, 2010, and 2020, and included geo-spatial techniques including the NSM, LRR, and WLR by using DSAS in the GIS environment. In addition, for the first time, the long-term shoreline position along the GC forecasted with the Kalman filter model was incorporated in DSAS. Given the resolution of the Landsat satellite images and the dynamic nature of the shoreline, this study should provide baseline information on the state of the shoreline in the GC and not the precise quantification and forecast of the shoreline.

Following this introduction, this paper was divided as follows: Section 2 illustrates the data and methods, and Section 3, the results and associated discussions. The conclusions of study the presented in Section 4.

2. Data and Methods

2.1. Study Area

The GC coast (31°30′ N, 114°48′ W to 22°00′ N, 105°40′ W) located in Northwestern Mexico extends along 4 states, Sinaloa, Sonora, Baja California, and Baja California Sur (Figure 1). The approximate length of the GC shoreline is 3370 km and provides important ecosystem services such as fisheries, tourism, and agriculture, which is why the population density along its coasts is increasing in the main ports. The GC has been integrated by RAMSAR sites and recognized since 2005 as a World Natural Heritage Site by the United Nations Educational, Scientific and Cultural Organization (UNESCO) [32].

Gulf ecosystems provide sufficient services to humanity and play a key role in achieving Sustainable Development Goals (SDGs). Achieving sustainability in coastal development comprises a combination of ecological, economic, and social elements [33]. The sustainability of gulf ecosystems worldwide is in a perilous state because of climatic and human-induced stresses [34], particularly in the GC.

The GC is not known for its powerful waves and strong currents [35], however, it is susceptible to tidal action, mainly in the upper Gulf, as it presents a shallow bathymetry, there are also mixed semi-diurnal tides, and there is one of the largest tidal ranges on earth at more than 3 km horizontally and 9 m vertically long [36]. Therefore, their coasts are highly variable even for short periods. On the coast of Baja California Sur, the beaches are of reduced extension, usually cut by cliffs and exposed to a low energy swell, except in the southern part where the energy is increased by the influence of the Pacific Ocean [37].

Several factors shape the dimensional or geometric characteristics of shorelines in the GC, one of the most important being increasing wave action [4], bathymetric changes, climate trends, and sea level rise. In addition, land use change and resource grabbing are alarming on the Gulf coast, as well as real estate development that has increased which has

eroded urbanized beaches. Breakwaters and jetties add to the modification of the shoreline. Therefore, adequate scientific and technical knowledge is required to preserve this great marine ecosystem [33].
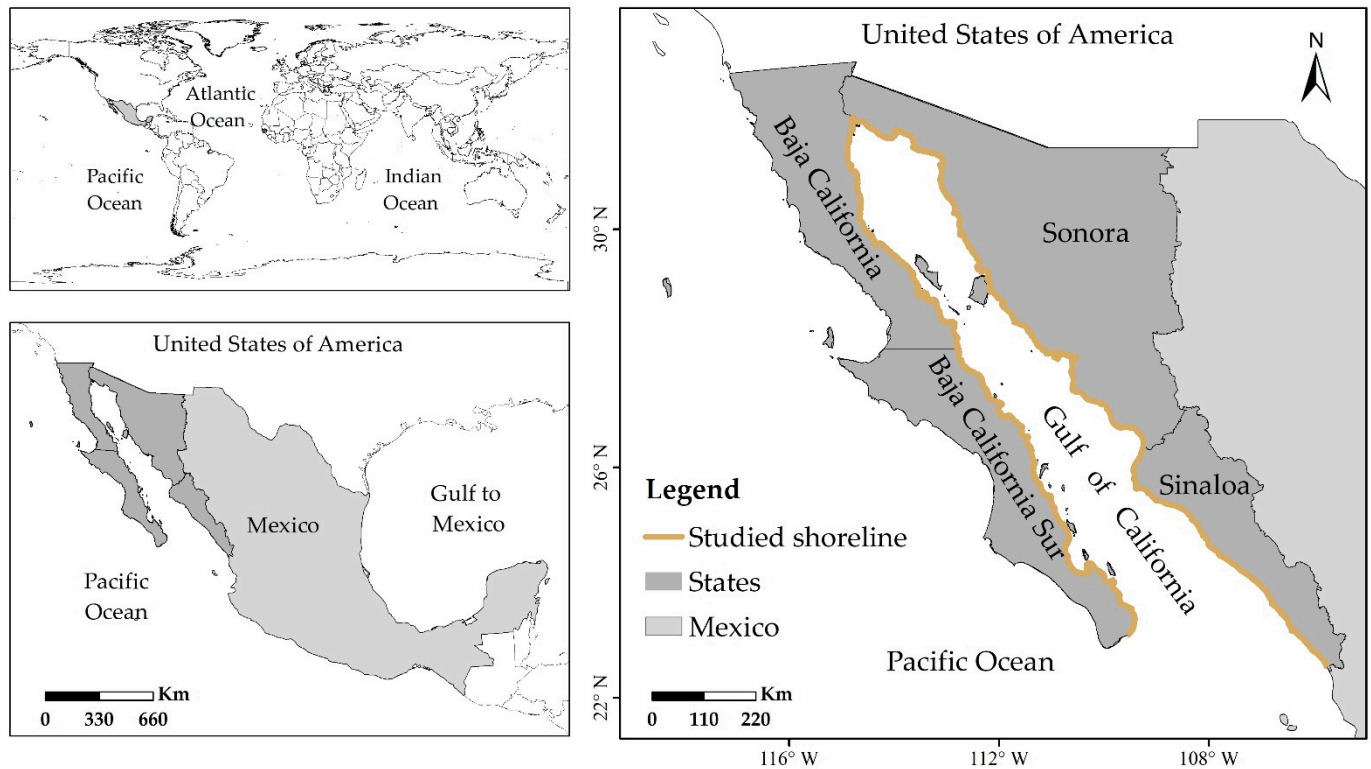

Figure 1. Study area location. Northwest Mexico, Gulf of California shoreline.

2.2. Methodology

Currently, remote sensing data are widely used depending on the purpose of use, as there are different satellite systems with a wide range of resolutions and other characteristics to be considered depending on their application. Commonly used Landsat satellite imagery is used in in coastal change studies because of its synoptic and repeatable coverage, high resolution, multispectral capabilities, and cost-effectiveness compared to conventional techniques [38]. This article follows the scheme shown in Figure 2 to evaluate the rate of coastal change and its forecast for 2030 and 2050, for which Landsat satellite images from five periods (Table 1) were acquired to extract the coasts of the GC between 1981 and 2020.

Table 1. Specifications of the satellite data.

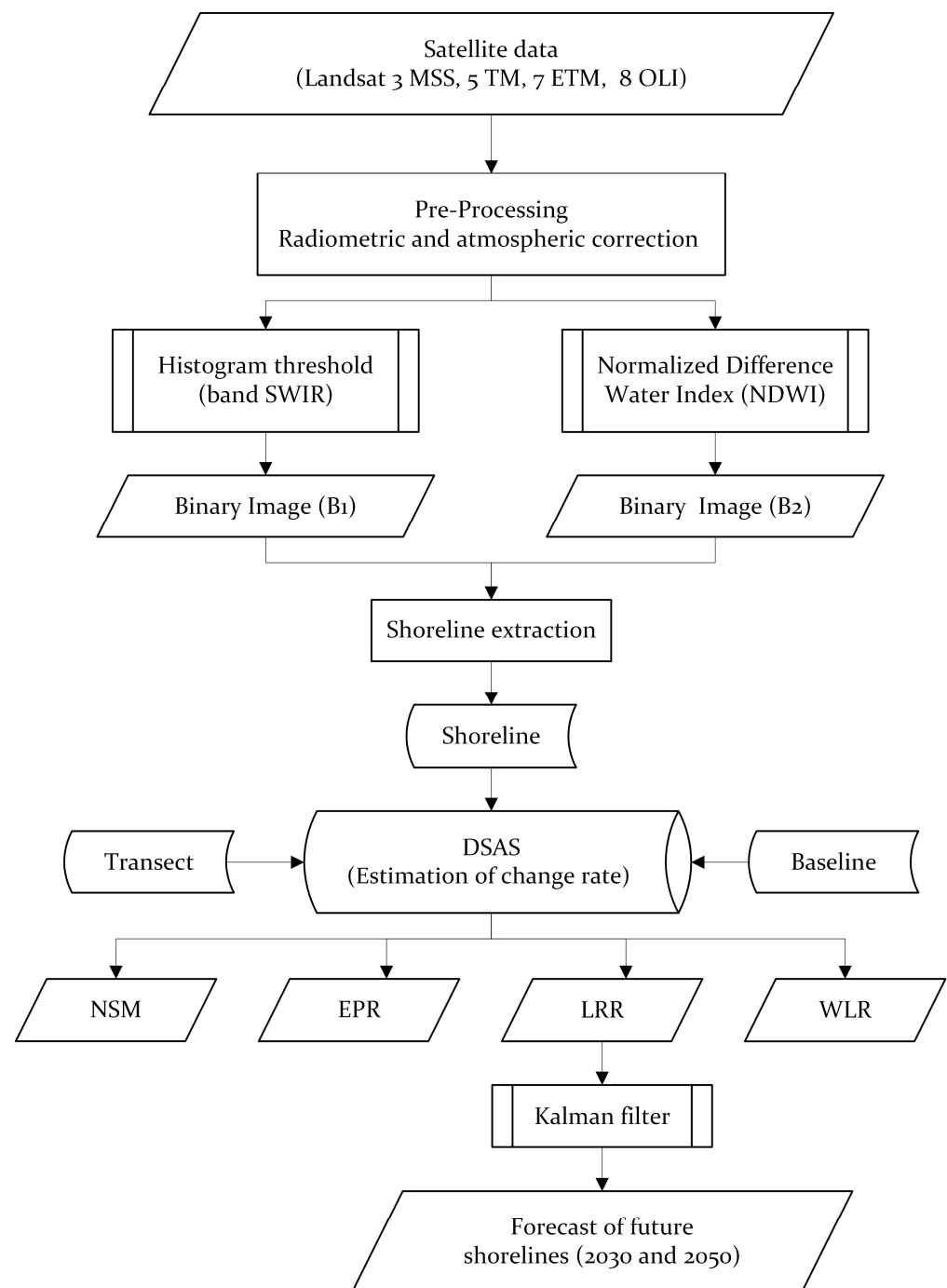| Satellite Data/Sensor	Year of Acquisition	Spatial Resolution (m)
Landsat 3-Multi-Spectral Scanner	1981	60
Landsat 5-Multi Spectral Scanner and Thematic Mapper	1993	30
Landsat 5-Multi Spectral Scanner and Thematic Mapper	2004	30
Landsat 7-Enhanced Thematic Mapper	2010	30
Landsat 8-Operational Land imager and Thermal Infrared Sensor	2020	30

Figure 2. Schematic representation of methodology.

2.3. Remote Sensing Image Preprocessing

This research used satellite images from the Landsat constellation (MSS, TM, ETM+, OLI), which were collected over approximately 40 years. The assessment of the shoreline variability started with the oldest year, 1981, which covered the entire coastal area of the GC, this being one of the fundamental requirements. Subsequently, the years with periods longer than ten years corresponding to 1993, 2004, and 2020 that also covered the GC coastal zone were selected, and the year 2010 was added to run the model with the forecast to 2020 and validate the results. To obtain cloud-free data and avoid other types of atmospheric and tidal errors, pre-monsoon satellite data for the months of March–April or after the September–October monsoon season worked [38]. Therefore, satellite images corresponding to October were downloaded, rectified, and projected to the World Geodetic

System (WGS 84), and the Universal Transverse Mercator (UTM) system [39], from the Earth Explorer website (https://earthexplorer.usgs.gov/, accessed on 21 March 2022) of the United States Geological Survey (USGS).

This study considered five shorelines, as the consideration of over two annual shorelines maintains greater accuracy in the calculation of the rates of change [40]. As stated in Goal 14 of the SDGs, accurate and continuous information on coastal positions is essential to coastal conservation [41]. However, reference changes, distortions from uneven contraction, stretching and folding, different topography and publication standards, projection errors and partial revision, etc., are potential errors associated with coastal mapping [42]. Mapping the shoreline with the lowest percentage error is always uncertain because of its variable and dynamic nature [8].

Radiometric correction of the images was required, i.e., converting digital numbers to reflectance values to compensate for the difference in the calibration of sensors from different satellites [39], subtracting inherent errors, and preparing a suitable image [21]. Therefore, the images were radiometrically and atmospherically corrected using ENVI 5.3 software by applying the Reflectance Radiometric Calibration module that combines the effects of the sun and the angle of view. Furthermore, sensor calibration with atmospheric correction [23] using the FLAASH module was used to correct for any atmospheric interference [43].

2.4. Shoreline Extraction

The following methods were used: (1) the single band threshold method, and (2) the Normalized Difference Water Index (NDWI), to obtain the shoreline following the method implemented by [29,39]. Minimal modification was made to the line taken by visual interpretation supported by the resulting NDWI images, which was taken as a support to define the line representing the wet–dry boundary as an approximation to the HWL [44–46], since it highlighted the upper limit of coastal wetting caused by the last high tide before the date of acquisition of the satellite image [46–48]. To improve the accuracy provided by the pixel size, this index used the Landsat green and NIR bands, expressed through the following equation:

$$NDWI = \frac{\lambda_g - \lambda_n}{\lambda_g + \lambda_n} \tag{1}$$

where λ_g = green band of Landsat data, λ_n = red band of Landsat data.

Finally, the shoreline was extracted by separating the land and water entities in the ArcGIS binary threshold tool [49]. The segmented binary image was converted to a vector image using the ArcGIS conversion tool and the shoreline boundary was extracted and converted to a shape file for further analysis.

2.5. Digital Shoreline Analysis System

DSAS v.5.1 was developed by the USGS in the early 1990s. This algorithm allows for obtaining change statistics from multiple historical shorelines, as well as a forecast of future shorelines [28]. It generates good performance results based on input features, such as the date and shape files from the shoreline. It is considered one of the most efficient and effective, as it provides a higher performance in the analysis of shoreline changes compared to other traditional tools and methods [38].

DSAS estimates the rate of change statistics for a time series of shorelines in vector format obtained from aerial photos, satellite imagery, or in situ measurements of shoreline positions. According to [28], the following is required:

(1) Creating a geodatabase within a Geographic Information System environment.
(2) Extracting the shorelines stated in Section 2.4.
(3) Constructing the baseline (Figure 3) in this study generated from the smoothing of the oldest line displaced 300 m offshore using the damping method. This method is the most reliable and accurate method for baseline demarcation [50].

(4) Generating transects perpendicular to the baseline. Creating 33,225 transects at 100 m intervals and a smoothing distance of 3000 m for Sonora and 2000 m for the rest of the states (Figure 3).

(5) Calculating the rates of change of the shoreline for which DSAS runs statistical models based on different measures between the historical positions of the shorelines for each of the transects, and generating different rates of change depending on the selected statistical methods [21].
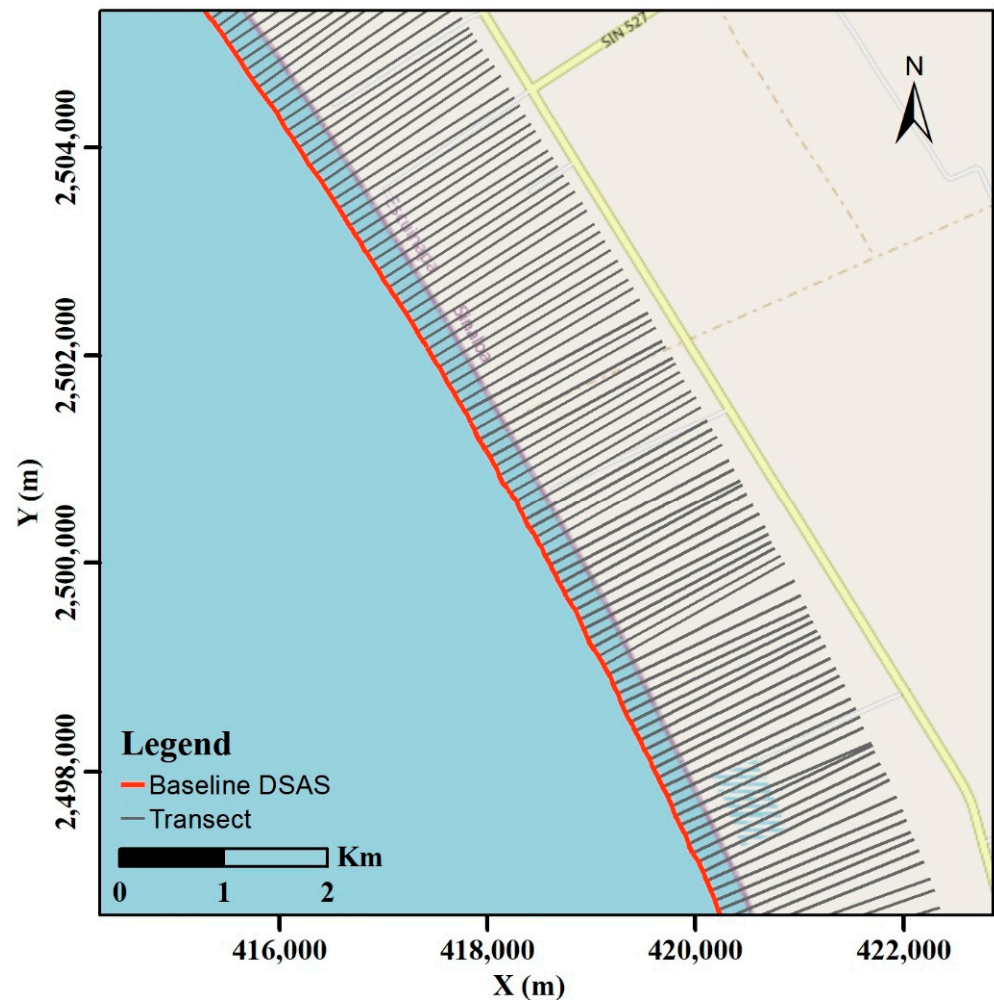

Figure 3. Example of transects and baseline.

The statistics used in this research are:

- Net Shoreline Movement (NSM) is the distance between the first and last shoreline. A statistical parameter calculated for each transect launched perpendicularly to the coast, [28] and represented by the following equation, where D is the distance in meters:

$$NSM = D_{new} - D_{old} \qquad (2)$$

- End Point Rate (EPR) is obtained by dividing the distance of the shore motion (NSM) by the time (T) elapsed between the oldest and most recent measurements in equation 3. The EPR is suitable for short-term coastal analysis between only two coasts [21,51].

$$EPR(m/yr) = \frac{NSM}{T} \qquad (3)$$

- Linear Regression Rate (LRR) comprises fitting the fewest squares regression line to multiple shoreline position points for a specific transect [28]. It is calculated by plotting the points where the coasts are intercepted by transects and calculating the linear regression, an equation:

$$Y = a + bx \tag{4}$$

  where Y is the distance in meters from the baseline, x is the coastal date interval in years, and b is the slope of the fitted line (m/year), i.e., the rate of change of the LRR shoreline, and as is the intersection. LRR is the line slope suitable for the long-term analysis of the shoreline change [51,52] and is based on accepted statistical concepts with satisfactory accuracy [38]. The next positions of the shoreline change were forecasted using this method [53].

- Weighted Linear Regression (WLR) determines a line of a better fit than the LRR, as it gives more weight to reliable data with a 95% confidence interval [54]. According to [54], the weight ω is defined as a function of the variance in the measurement uncertainty (e), and the weighting value ω is linked to the shore data before examining its rate of change [21].

$$\omega = \frac{1}{e^2} \tag{5}$$

- WLR considers ambiguity at each shoreline position when calculating a trend line. The weight assigned to each shore position is the inverse of the squared positional uncertainty. Therefore, the shorelines with higher uncertainty have less influence on the trend line than data points with higher uncertainty [38].

The selected statistics provide an understanding of the changes in the shoreline over the years, such as NSM representing the distance the shoreline has advanced/receded over, while the EPR, LRR, and WLR represent erosion rates. This method was selected to determine the long-term rates of change and represent the results, as they can effectively simulate the spatial and temporal rates of change on the coast [10].

The coasts are dynamic, and present changes in coastal erosion or accretion. The classification proposed by [4] was used to represent the rates of change. All positive values represent a seaward movement of the coast (accretion), and negative values show landward movement (erosion) [38,51].

The rates of change were classified considering that the Landsat images used to have a resolution of 30 m per pixel. Considering this and the period analyzed, a margin of error was obtained for the units of the rates of change (m/year) [55].

Uncertainty Estimation

The accuracy of the shoreline position, as well as rates of change, can be influenced by several sources of error, such as the tide level position, digitizing error, resolution, and image registration [21,38]. *Unc*, the uncertainty value of each of the shorelines considers these positional and measurement errors, expressed by the equation:

$$Unc = \sqrt{\left(E_s^2 + E_{td}^2 + E_d^2 + E_r^2 + E_p^2 \right)} \tag{6}$$

where E_s^2 are seasonal errors, E_{td}^2 is the tidal fluctuations error produced by the HWL error, E_d^2 is the digitizing error, E_r^2 is the rectification error, and E_p^2 is the pixel error. This approach assumes that the component errors are normally distributed [56]. These uncertainties were used as weights in the change rate calculations. The value was annualized to provide an error estimate (E_{EPR}) for the rate of shoreline change at any given [21,28,38,57] transect using the following equation:

$$E_{EPR} = \frac{\sqrt{Unc_1^2 + Unc_2^2 \ldots Unc_n^2}}{Date_n - Date_1} \tag{7}$$

where Unc_1, Unc_2, and Unc_n denote the total uncertainty of the shoreline position for the various years analyzed, $Date_n$ is the year of the latest shoreline, and $Date_1$ is the year of the oldest shoreline.

2.6. Shoreline Forecast (2030, 2050) and Model Validation

For forecasting, the Kalman filter model [58] incorporated in DSAS used required historical shoreline position data [28] to combine the observed lines with the model-derived positions and forecast a future shoreline position [59]. This Kalman filter is statistically based and requires a set of linear regression rates to initialize the values in the model and accurately forecast the future position of the coast. This filter is run to minimize the observed error between the model and shore positions when running the forecast [28,59].

The model used the oldest shoreline to forecast the position of the subsequent shoreline and found the sequential step repeated until the next shoreline position. Each time it reached a new shoreline position, it performs the validation process between the modeled and the observed shoreline by updating the rate and uncertainties to improve the forecast model. The updated rates worked and were repeated until the chosen forecast date was reached [21]. The model builds estimation areas, performs rate calculations providing factual information to assess the robustness of the rates, and incorporates a beta model of the shore determination with ambiguity bands [28]. However, it should be noted that the Kalman filter model applies a quantitative analysis of the long-term migration pattern of the coast to forecast the future position of the coast, considering that the same factors would be involved as in the past.

The shoreline forecasted for the years 2030 and 2050 used the historical shoreline positions from 1981 to 2020. Since this model incorporated in DSAS requires validation, validation was performed by comparing the forecasted line to the year 2020 using the historical shoreline position from 1980, 1993, 2004, and 2010. Subsequently, the position of the extracted and forecasted 2020 shoreline was compared to calculate the RMSE error of the positional difference between them by:

$$RMSE = \sqrt{\left\{ \left(X_p - X_r \right)^2 + \left(Y_p - Y_r \right)^2 \right\}} \tag{8}$$

where X_p and Y_p are the forecast model coordinates of the coast, and X_r and Y_r are the actual coordinates of the shoreline.

In addition, the value of the regression coefficient was calculated using a scatterplot based on the LRR output of the actual and model-derived shorelines.

3. Results and Discussions

3.1. Shoreline Change Analysis between 1981 and 2020

The analysis of the shoreline over the 40 years using geospatial and statistical techniques contributed to a better understanding of the coastal variability along the GC. The performance of the shorelines for the years 1981, 1993, 2004, 2010, and 2020 were incorporated in the geodatabase, as well as the baseline and a total of 33,225 transects along the GC, of which 5937 were for Sinaloa, 10,906 for Sonora, 6293 for Baja California (BC), and 10,089 for Baja California Sur (BCS). All transects were cut from the baseline to the farthest line, as shown in (Figure 4).
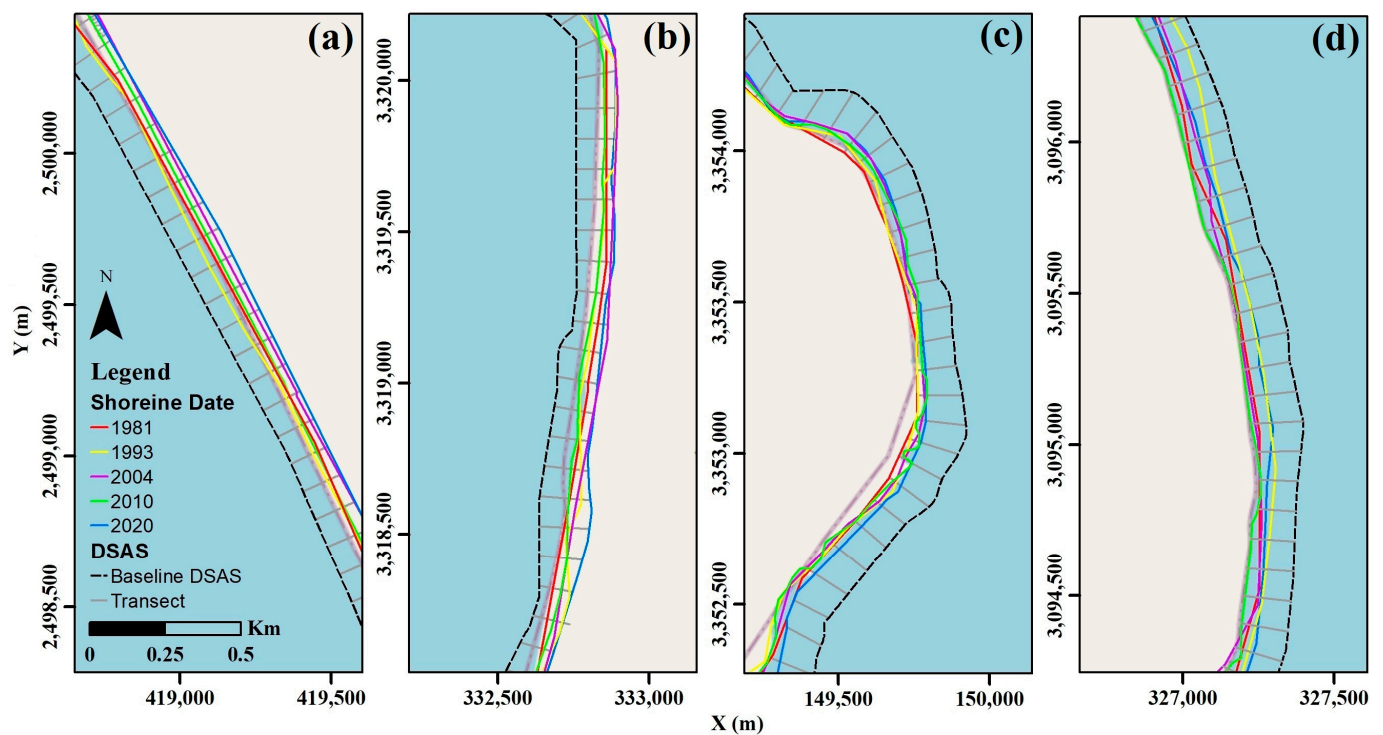
Figure 4. Shoreline: (**a**) Sinaloa, (**b**) Sonora, (**c**) Baja California, and (**d**) Baja California Sur.

The statistical models NSM, EPR, LRR, and WLR were obtained for a better understanding of the movements of the shoreline up to the present time. Considering the resolution of the image and the period analyzed, an uncertainty range for the rate of change in units of 0.75 m/year resulted. Because of the uncertainties, the results were obtained from the rate of change of the coast from the LRR with a confidence level of 95%.

The results of the shoreline movement revealed that there was significant landward (erosion) and seaward (accretion) movement in different sectors of the GC, and this can differ greatly between the coastal stretches, which can range from more than 1 km to tens of kilometers [55]. Table 2 details the displacements in terms of the NSM and provides detailed information on the movements that occurred. Along the coasts, there were 22,295 transects with landward movement and 10,930 seaward movements. The longest landward distance was −2880.39 m on the coast of Sonora, while the longest positive seaward distance was 1325.71 m on the coast of Sinaloa.

Table 2. Shoreline changes by NSM.

Statistics	Sinaloa	Sonora	BC	BCS	GC
Number of transects	5937	10,906	6293	10,089	33,225
Average distance (m)	−39.61	−176.9	−105.46	−4.32	−81.57
Number of transects with a negative distance	4417	9558	2749	5571	22,295
Maximum negative distance (m)	−515.90	−2880.39	−1650.21	−176.94	−2880.39
Average of all negative distances (m)	−105.48	−210.54	−281.73	−30.95	−157.17
Number of transects with a negative distance	1520	1348	3544	4518	10,930
Maximum positive distance (m)	1325.71	747.76	278.6	318.92	1325.71
Average of all positive distances (m)	116.424	65.2	37.64	29	62.06

The EPR statistical analysis revealed that the changes were significant throughout the GC, which presented a rate of change of 2.16 m/year (Table 3), similar to that reported by [4], who analyzed the shoreline variability with EPR in the GC. The EPR does not consider the variability between all the shorelines since it considers only the oldest and the current line. Therefore, in this research, we discuss the results in terms of the LRR

to account for all shorelines in the analyzed period and compared them with the results of WLR.

Table 3. Shoreline change rates by EPR.

Statistics	Sinaloa	Sonora	BC	BCS	GC
Average rate (m/year)	−1.32	−4.56	−2.69	−0.09	2.16
Maximum value erosion (m/year)	−26.54	−118.36	−42.83	−29.93	−118.36
Average of all erosional rates (m/year)	−3.23	−5.44	−7.39	−0.76	−4.20
Maximum value accretion (m/year)	66.09	40.25	7.21	16.58	66.09
Average of all accretion rates (m/year)	4.24	1.63	0.97	0.74	1.89

The LRR results (Table 4) indicate an overall rate of change of −2.20 m/year. A total of 72% percent of coasts with landward advancement with an erosion rate of 3.86 m/year, while 28% demonstrated seaward gain with a rate of 2.05 m/year.

Table 4. Shoreline change rates by LRR.

Statistics	Sinaloa	Sonora	BC	BCS	GC
Average rate (m/year)	−1.58	−4.57	−2.35	−0.31	−2.20
Percent of all transects that are erosional (%)	78.64	88.05	47.83	66.14	72.19
Percent of all transects that have statistically significant erosion (%)	33.54	36.36	3.91	10.14	21.91
Maximum value erosion (m/year)	−20.87	−118.02	−46.27	−5.92	−118.02
Average of all erosional rates (m/year)	−3.33	−5.42	−5.88	−0.83	−3.86
Percent of all transects that are accretion (%)	21.36	11.95	51.17	33.86	27.62
Percent of all transects that have statistically significant accretion (%)	5.12	1.84	5.13	3.14	3.46
Maximum value accretion (m/year)	55.21	18.34	6.54	6.43	55.21
Average of all accretion rates (m/year)	4.89	1.75	0.89	0.7	2.05

With WLR, it assigns a higher weight to transect the intersection points with lower uncertainty values to obtain the line of best fit. However, the WLR values (Table 5) differ in centimeters from the LRR in the study. The overall rate of change for the WLR for the Gulf was −1.78 m/year, demonstrating a difference of 0.42 concerning the LRR. For this reason and the forecast of the futuristic position of the coast obtained from the LRR results, this research discusses the results mainly in terms of the LRR.

Table 5. Shoreline change rates by WLR.

Statistics	Sinaloa	Sonora	BC	BCS	GC
Average rate (m/year)	−1.12	−3.69	−1.89	−0.45	1.78
Percent of all transects that are erosional (%)	68.87	77.84	53.54	69.38	69.06
Percent of all transects that have statistically significant erosion (%)	18.41	22.14	1.57	7.54	13.21
Maximum value erosion (m/year)	−32.27	−130.32	−37.74	−28.1	−130.32
Average of all erosional rates (m/year)	−2.91	−5.32	−2.77	−1.02	−3.00
Percent of all transects that are accretion (%)	31.13	22.16	46.46	30.62	30.93
Percent of all transects that have statistically significant accretion (%)	5.51	1.12	2.19	1.71	2.32
Maximum value accretion (m/year)	64.04	60.61	6.20	36.13	64.04
Average of all accretion rates (m/year)	3.74	2.06	0.82	0.82	1.86

Among the main factors that change the shoreline are tidal currents, wave patterns, bathymetric changes, climate trends, sea level rise, land use change, and resource grabbing, as well as other anthropogenic elements such as breakwaters, jetties, among others, that add to the modification of the shoreline [60]. Human interference in the natural process with agricultural and aquaculture activities involving the construction of tide gates and the dredging of channels is also important [26]. Another relevant factor to consider is the decrease in sediments that reach the sea because of the damming of rivers that change

the natural channel, producing changes that affect sedimentation rates or loss because of coastal transport and generate changes to the shoreline [61,62]. Therefore, the results of erosion or accretion in this research cannot be attributed to a specific factor or only to environmental processes (seasonal, interannual, and decadal climate variability), climate change, and anthropogenic processes, in agreement with [4,26,55]. Currently, this problem is not only present on the coast of the GC in Mexico, but throughout the world, in countries such as China, Japan, Chile, the United States, Argentina, and Russia, where more than half of the coast has transformed because of erosion and land use, which has had a significant impact on the coastal processes and sediment supply.

3.2. Analysis by State

Along the coast of Sinaloa, 4417 transects have negative distances and 1520 positive. The largest landward movement was 515.90 m, and the greatest seaward movement was 1324.71 m (Figure 5a and Table 2).
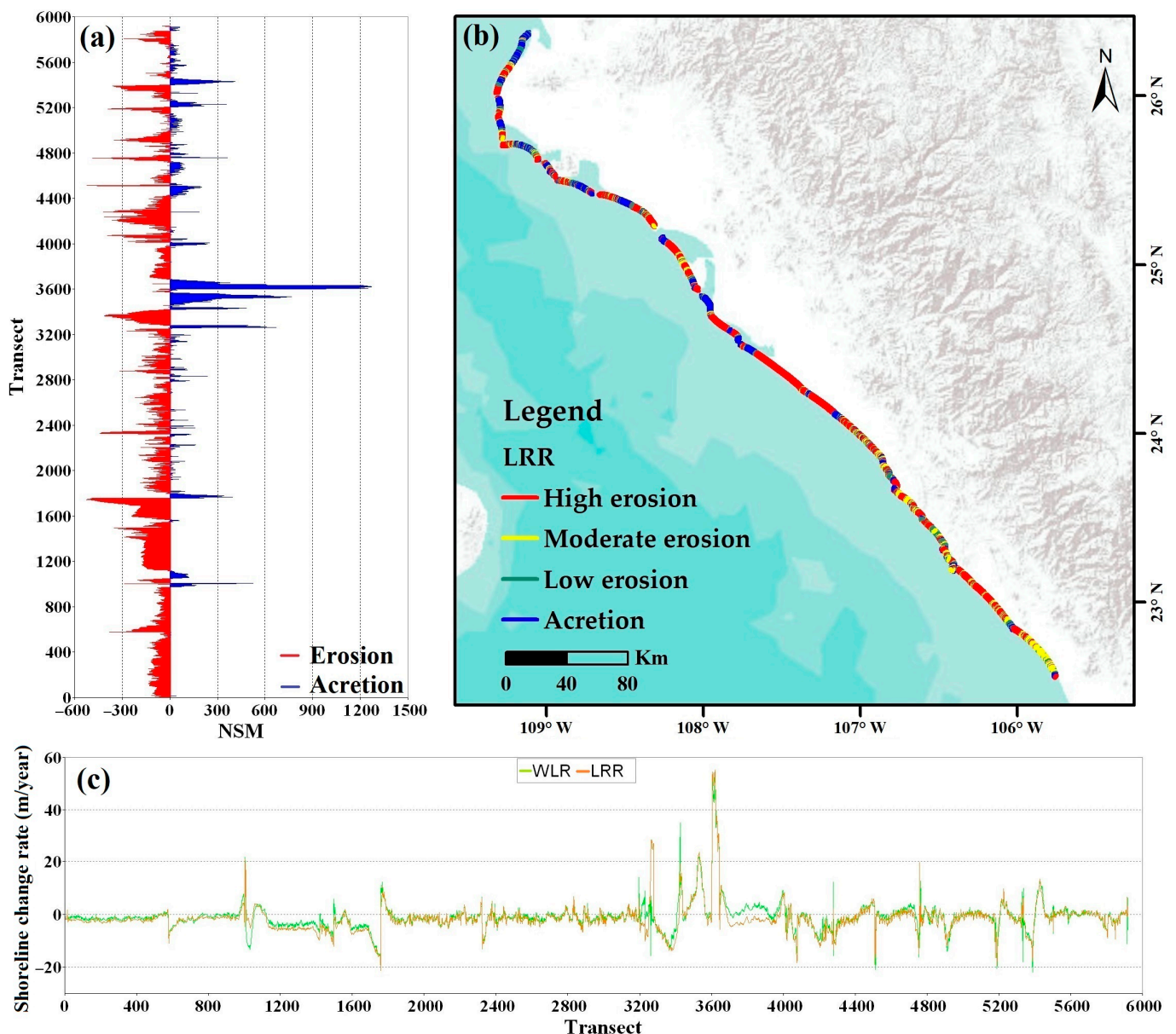

Figure 5. Shoreline dynamics and evaluation, (**a**) NSM (m), (**b**) LRR (m/year), and (**c**) WLR (m/year) along Sinaloa.

The result of the LRR statistic (Figure 5b and Table 4) shows that Sinaloa presented with constant erosion with an overall rate of change of −1.58 m/year along its coast. Seventy-eight percent of the shoreline is eroding at an average rate of −3.33 m/year. The rest of the shoreline is accreting at an average rate of 4.89 m/year. A maximum erosion and accretion rate of −20.87 and 55.21 m/year, respectively, were observed. Though WLR presented with an overall rate of change of −1.12 m/year (Table 5), lower than that of LRR, it followed a similar trend to the LRR (Figure 5c).

A large portion of Sinaloa is shoreline that has experienced erosion, largely attributed to the construction of dams on a majority of its rivers, which has resulted in a retention of sediments that would have otherwise reached the ocean [61]. This phenomenon has eroded, occurring predominantly at the mouths of these rivers. Another reason that the Sinaloa coast is highly eroded is that it is subjected to constant meteorological phenomena because it is in a natural tropical cyclone corridor. This situation increases the variability in the shoreline, resulting in short-term erosion caused by these phenomena, which sometimes remain permanent, affecting both the coastal system and the infrastructure near the shoreline.

Sinaloa has anthropogenic activities along the shoreline that directly and indirectly affect the contribution of sediments, such as breakwaters, jetties, and dams, besides the construction of protection and productive activities, since 80% of the state population is near these coastal environments. The impact of these structures makes the coastal zone more vulnerable to erosion, a fact that coincides with the research conducted by [62].

In Sinaloa, there are some coastal investigations in more specific areas such as those performed in Las Glorias beach. Data from this research show that it is already highly eroded, similar to what was reported by [29] where they analyzed the historical changes of the shoreline to find the main drivers of change and its risk to coastal erosion, finding an overall rate of change of −5.4 m/year. Jimenez-Illescas et al. [33] found that Las Glorias Beach has lost up to 300 m perpendicular to the coast along its 4.5 km length and suggested the use of geo-tubes to lessen the problem. Other beaches such as Mazatlán have suffered erosion at a rate of −1.9 ± 0.9 m/year during the last decade [63], data similar to those obtained in this study. Coastal variability also affected the coastal lagoon system such as that of Topolobampo, because of tidal hydrodynamics at that location, even though this system exports sediments to the GC [64].

While Sonora presented 9558 transects with negative distances and a maximum landward movement of −2880.39 m, 1348 had positive distances and a maximum seaward movement of 747.76 m (Figure 6a and Table 2).

The coast of Sonora presented a general rate of change LRR of −4.57 m/year; it was the state with the most variability on its shoreline. These results show that 88% of its shoreline is undergoing erosion with an average rate of −5.42 m/year. Meanwhile, the rest is undergoing accretion with an average rate of 1.75 m/year, and a maximum erosion and accretion rate of −118.08 and 43.12 m/year, respectively (Figure 6b and Table 4). The rate of change for WLR was −3.69 m/year (Table 5), with a similar trend to the LRR with a difference of 0.88 (Figure 6c).

Unlike Sinaloa, Sonora has very high erosion north of its coast. This is attributed mainly to the damming of the Colorado River, which has the most influence since the sediments and nutrients that used to reach the sea are now dammed in the reservoirs of the dams. The Colorado River reduced its discharge to inconsequential volumes after the construction of Hoover Dam in 1968 and the increase in demand for irrigation [65]. Thus, human intervention in the Colorado River watershed has eliminated water discharge and almost all sediment supply to the river mouth and delta [66], resulting in sediment starvation throughout the Northern GC [67]. Agreeing with Laksono F. et al. [62], the persistent decline in the river sediment supplies due to water harvesting for human and agricultural use causes the significant loss of beach areas. The marine environment of the Upper GC has semi-diurnal and diurnal tidal cycles, with wide variations in the sea level ranging from 6.95 m in San Felipe to about 10 m in the Colorado River delta [36,65]. In this region, the sediment dispersal, transport, and deposition are now controlled primarily by

oceanic forcing rather than by fluvial processes, as was in the past [65]. This is in addition to the anthropogenic effects on coastal areas generated by residential tourism in coastal destinations in Northwestern Mexico, including Puerto Peñasco [68].
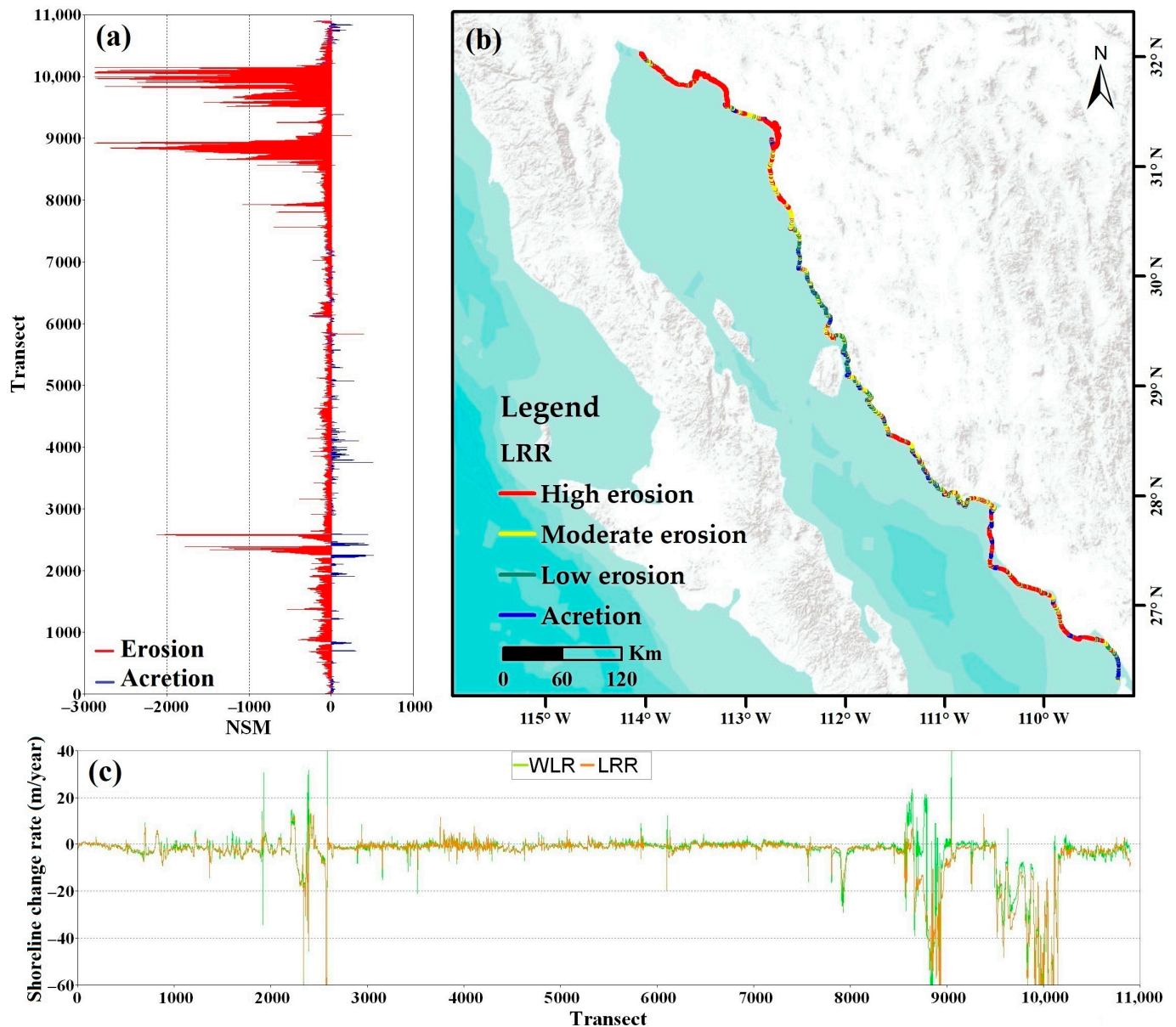

Figure 6. Shoreline dynamics and evaluation, (**a**) NSM (m), (**b**) LRR (m/year), and (**c**) WLR (m/year) along Sonora.

In the case off on the coast of Baja California, 2749 transects had negative distances and 3544 positives. The most landward movement was −1650.21 m, and the maximum seaward movement was 278.6 m (Figure 7a and Table 2).

The LRR presented an overall rate of change of −2.35 m/year, 47.8% of the coast presented erosion with an average rate of 5.88 m/year, and 51.2% of the coast presented accretion with an average rate of 0.89%. The maximum observed rate of erosion and accretion was −46.27 and 6.54 m/year, respectively (Figure 7b and Table 4). The overall rate of change WLR was −1.89 m/year (Table 5) with a similar trend to LRR along the coast (Figure 7c).
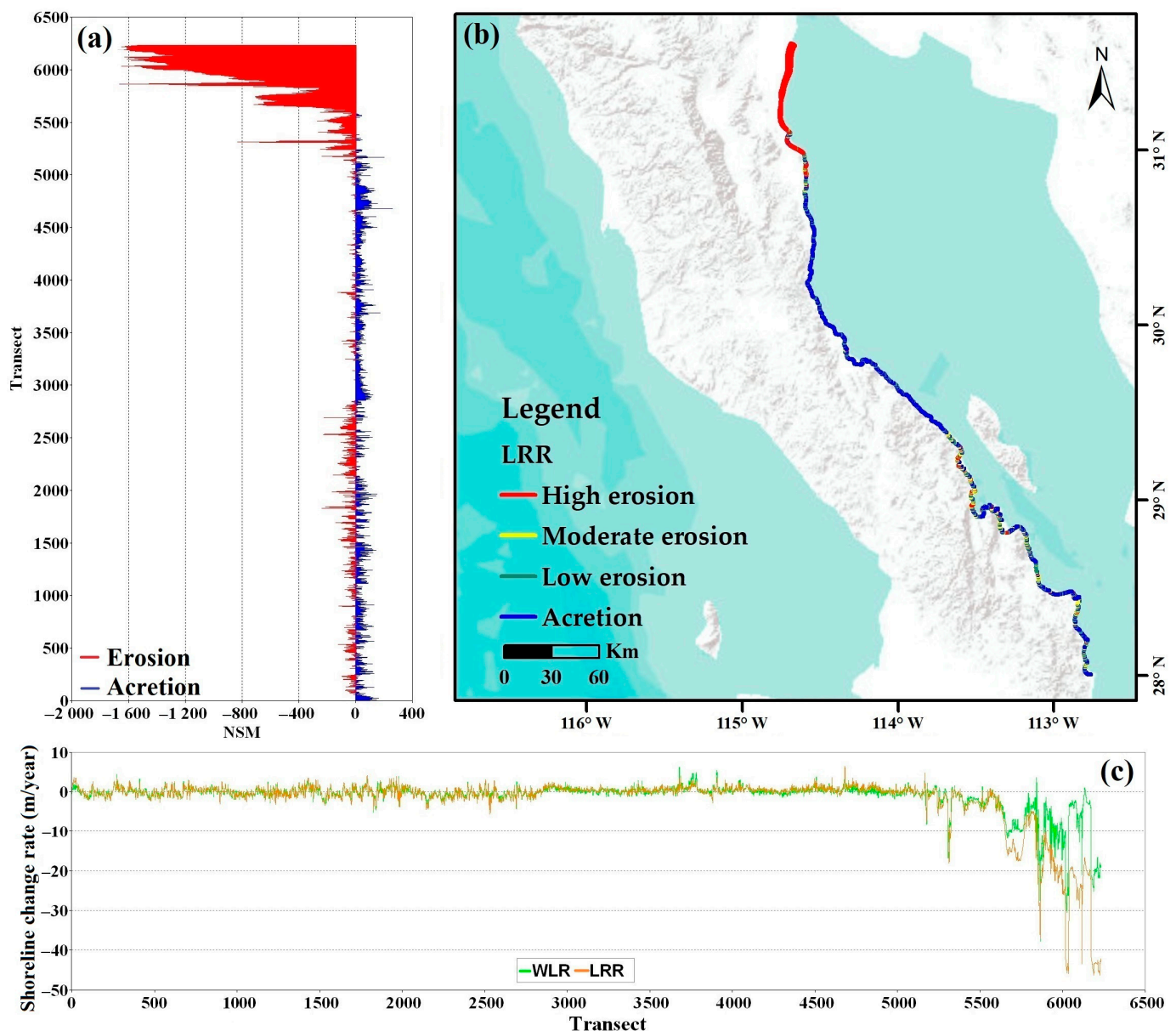
Figure 7. Shoreline dynamics and evaluation, (**a**) NSM (m), (**b**) LRR (m/year), and (**c**) WLR (m/year) for Baja California.

For Baja California, the results showed that the Upper Gulf coast is dominated by significant erosion, which can mainly be attributed to human activities, one of the most notable being the construction of over 20 dams along the Colorado River since the 1930s [67,69], reducing the freshwater flow basically to zero. The Colorado River is used to supply fresh water and silt [69]. Currently, the sediments that reach the coast are minimal, making it more sensitive to variations in physical conditions [67]. Therefore, the variability in the shoreline could no longer be attributed to whether sediments arrive, but to its mechanism, which would already depend on the oceanic forcing in that area [65].

On the other hand, Baja California Sur presented 5571 transects with negative distances and a maximum landward movement of −176.94 m. A total of 4518 had a positive distance with a maximum seaward movement of 318.92 m (Table 2).

The results reveal that the coast of Baja California Sur is the most stable, in contrast to the other states (Figure 8a). Its overall rate of change was −0.31 m/year. The results show that 66.14% of the shoreline is undergoing erosion with an average rate of −0.83 m/year, while the rest is undergoing accretion with an average rate of 0.7 m/year, and a maximum

erosion and accretion rate of −22 and 14.32 m/year, respectively (Figure 8b and Table 4). The WLR presented an overall rate of change of −0.45 m/year (Table 5) with a trend very similar to the LRR with a difference of 0.14 (Figure 8c).
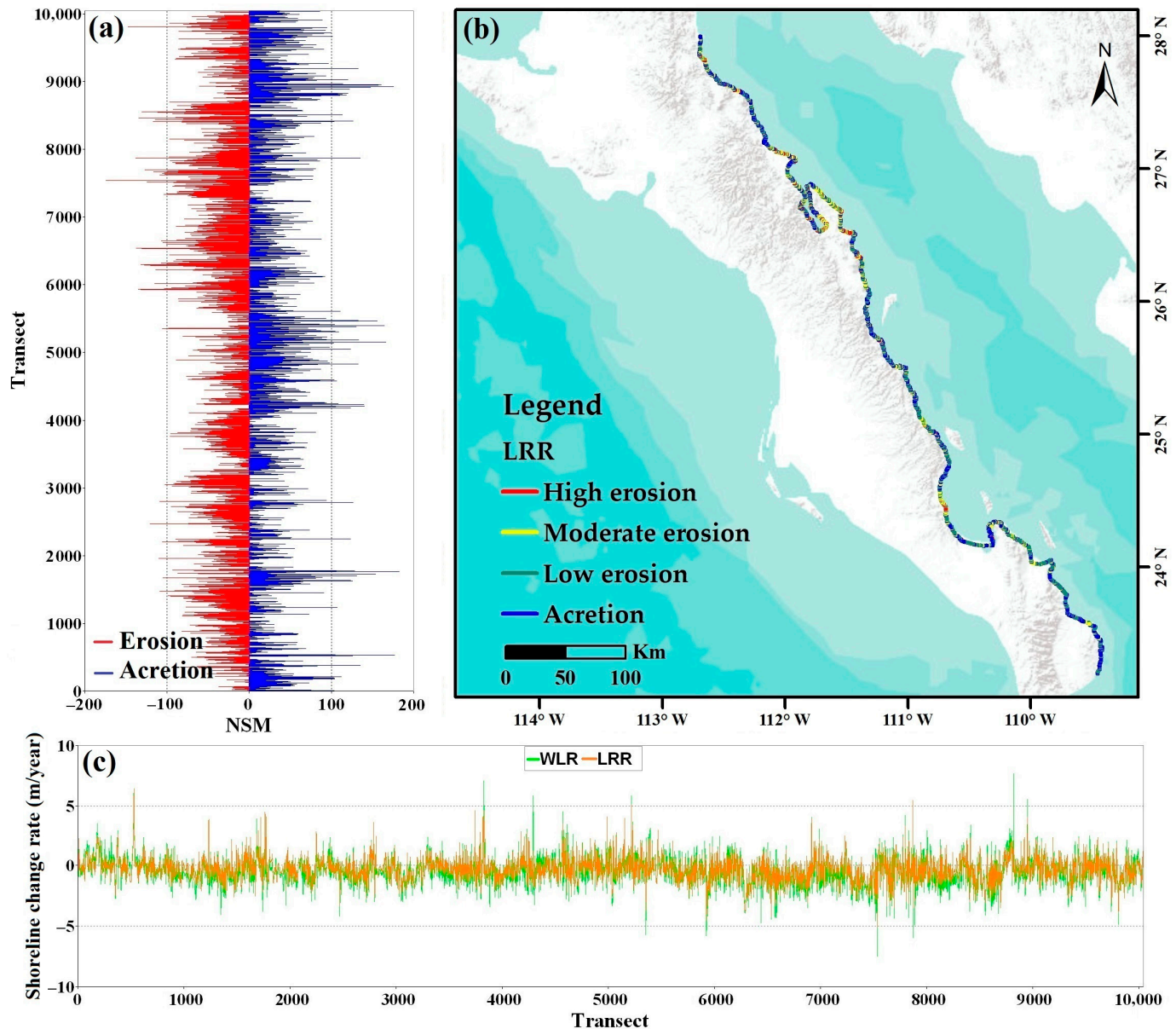

Figure 8. Shoreline dynamics and evaluation, (**a**) NSM (m), (**b**) LRR (m/year), and (**c**) WLR (m/year) for Baja California Sur.

The main attributed factors responsible for the beach variability in Baja California Sur are due to climate change, which causes an increase in the wave energy and a more frequent occurrence of tropical cyclones, generating periods of erosion and accretion, consistent with the probable causes of coastal erosion in the research conducted on the Pacific coast of Panama [27]. Although the anthropic impact is locally significant, as in Santa Rosalia, Loreto, and La Paz, since any modification of the natural sedimentary system can erode or cause accretion of the shoreline, the impact of the natural sedimentary system can be significant [37]. There is some research on the analysis of changes to its coasts, e.g., [70], which estimated the accretion and erosion rates of the Punta Arena in Los Cabos from Landsat satellite images for 1984–2016. In Puerto Escondido, barrier rock deposits were

examined that close lagoons as the outcome of lateral transport from adjacent rocky shores subject to recurrent storm erosion [71].

3.3. Future Shoreline Forecast and Model Validation

This research forecasts the future position of the shoreline for the years 2030 and 2050, to understand the future dynamics of the coast. The period from 1981 to 2020 was used to forecast the shorelines, and the linear regression method and the application of the Kalman filter were chosen. The shoreline forecast with the LRR model showed significant shoreline setbacks (Figure 9) and revealed the same pattern as the coastline changes between 1972–2020. Such a pattern was also observed along the coast of Catania, Southern Italy [62].
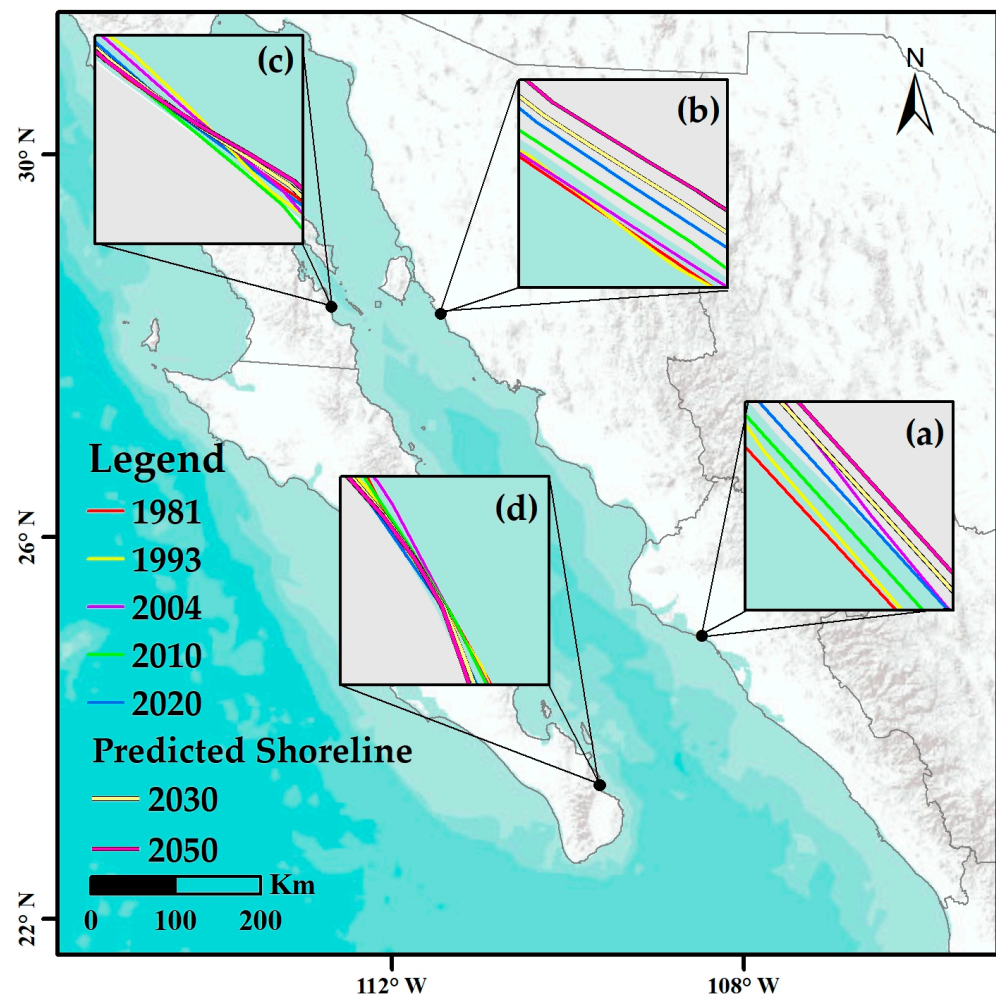

Figure 9. Current shoreline (2020) and forecast shorelines for 2030 and 2050, (**a**) Sinaloa, (**b**) Sonora, (**c**) Baja California, and (**d**) Baja California Sur.

The results showed that erosion will occur continuously throughout the GC for the forecasted year, observing mainly significant setbacks at river mouths and in highly urbanized coastal areas. This is a consequence of the lack of protection and mitigation measures. These also coincide with the same factors that are attributed to the coast of Oaxaca, Mexico, which affect the dynamics of the coast, mainly affecting ports and beaches [21]. Any coastal activity and development will have an indirect impact on the shoreline changes, and at the same time, the coastal community would face a serious problem in the future in the case of continuing with the same growth rate of the erosion. In addition, the biophysical conditions of the coastal environment would be degraded [26]. The results revealed that more than 70% of the shoreline will continue to recede along the GC.

Validation of the model accuracy was performed with the 1981, 1990, 2000, and 2010 shoreline, with which the 2020 shoreline forecasted and compared to the actual 2020 shoreline that resulted in an overall RMSE of ±7.43 m was used to validate, compare, and estimate the error of the model output and finally forecast the future shoreline. This was especially important for areas close to rivers and harbors, which are likely to be strongly influenced by factors such as anthropogenic and fluvial sedimentation as [62] mentions. In addition, the sea level rise, rainfall, river discharge, storm, wave dynamics, and tidal dynamics along estuarine and wetland areas are important factors influencing future shorelines [21]. For the upper Gulf, the forecast appears much more irregular than the original position. However, in over 90% of the coast, the forecast shoreline is within the default uncertainty band buffer value, a result comparable to what we obtained in [28].

In addition, a scatterplot and regression diagram was performed based on the data obtained from the LRR of the real and model-derived shorelines for each state (Figure 10), where it observed that there is a strong relationship between the LRR, since the R^2 was greater than 0.78 in all four states. This was also performed for the whole GC, obtaining an R^2 value of 0.95. This shows that there is a strong relationship between the actual shoreline and the forecasted shoreline.
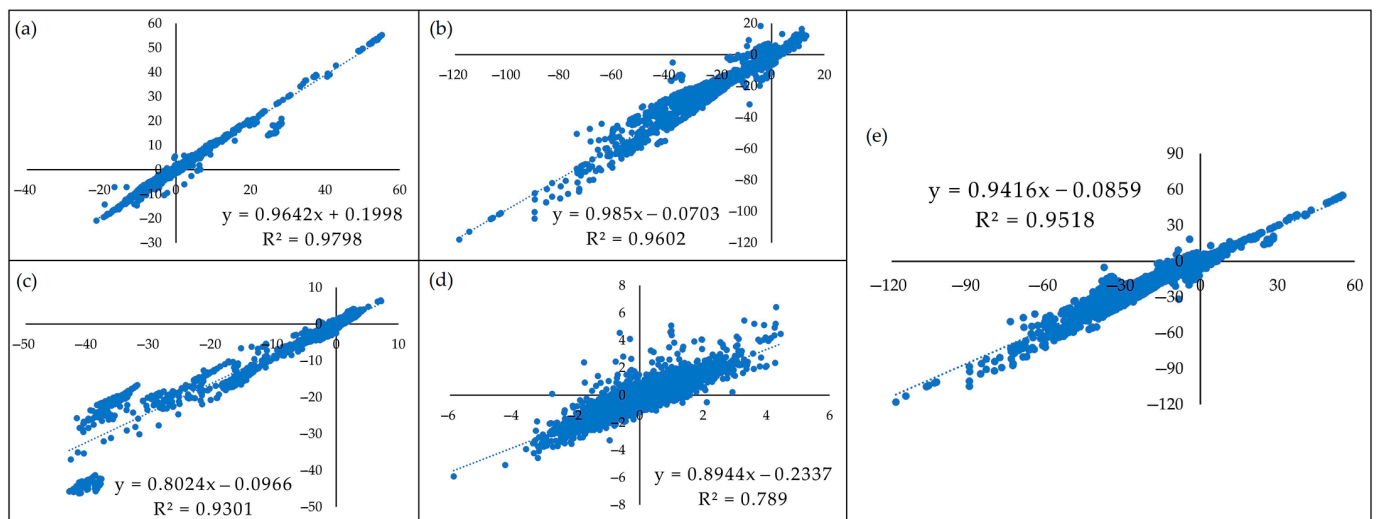

Figure 10. LRR change for the original and forecasted 2020 shoreline, (**a**) Sinaloa, (**b**) Sonora, (**c**) Baja California, (**d**) Baja California Sur, and (**e**) GC.

4. Conclusions

The shoreline changes along the coast of the Gulf of California between 1981 and 2020 were analyzed, and the shoreline positions for the years 2030 and 2050 were forecasted. Based on the extraction of the shoreline data from Landsat satellite images and the application of geospatial techniques and a shoreline forecast algorithm incorporated in DSAS, the following inferences were drawn.

The results showed that approximately 72% of the Gulf of California shoreline is undergoing steady erosion, and 28% is subject to accretion. Sonora had 88% of its shoreline eroding at a rate of −5.42 m/year, with greater retreats on the upper Gulf coast. Seventy-eight percent of the coast of Sinaloa presented erosion with a rate of −3.33 m/year, while the coasts of Baja California and Baja California Sur presented erosion in 48% and 66% of their coasts, with rates of −5.88 m/year and −0.83 m/year, respectively. The coast that showed the greatest stability was Baja California Sur, with an overall rate of change of 0.32 m/year, while the most unstable was Sonora, with an overall rate of change of 4.57 m/year.

The model for forecasting the future position of the shoreline indicated that the lines will continue to recede. The mapping, monitoring, and forecasting changes in the coast using multi-temporal satellite imagery and the application of the DSAS model along the

Gulf of California coast could be crucial in formulating mitigation policies and regulations, as the results provide a better understanding of the historical change that the shoreline has undergone, as well as its future prognosis.

Although this study did not examine the exact causes of the observed shoreline changes, they can be attributed to natural processes, human activities, and climate change, which are compelling the landward movement of shoreline positions. With the forecast of a spatial and temporal erosion trend in the shoreline changes, there is an urgent need for follow-up research in coastal areas where significant shoreline retreat is occurring, and for coastal risk management policies that take this reality into account.

Author Contributions: Conceptualization, Y.G.Z.-M., W.P.-R. and C.F.-O.; Methodology, Y.G.Z.-M., W.P.-R. and C.F.-O.; Validation, Y.G.Z.-M. and S.A.M.-A.; Formal analysis, Y.G.Z.-M., W.P.-R., S.A.M.-A. and C.F.-O.; Investigation, Y.G.Z.-M., W.P.-R., S.A.M.-A. and C.F.-O.; Resources, Y.G.Z.-M. and C.F.-O.; Data curation, Y.G.Z.-M.; Writing—original draft, Y.G.Z.-M., W.P.-R. and C.F.-O.; Writing—review & editing, Y.G.Z.-M., W.P.-R., S.A.M.-A. and C.F.-O.; Visualization, Y.G.Z.-M. and S.A.M.-A.; Supervision, W.P.-R., S.A.M.-A. and C.F.-O.; Project administration, C.F.-O.; Funding acquisition, C.F.-O. All authors have read and agreed to the published version of the manuscript.

Data Availability Statement: The new data created in this study are available on request.

Conflicts of Interest: The author declares no conflict of interest.

References

1. Boak, E.H.; Turner, I.L. Shoreline Definition and Detection: A Review. *J. Coast. Res.* **2005**, *214*, 688–703. [CrossRef]
2. Sevilla, N.P.M.; Adeath, I.A.; Le Bail, M.; Ruiz, A.C. Coastal Development: Construction of a Public Policy for the Shores and Seas of Mexico. In *Coastal Management: Global Challenges and Innovations*; Academic Press: Cambridge, MA, USA, 2018; pp. 21–38. [CrossRef]
3. National Commission for the Knowledge and Use of Biodiversity. Cartography of the Mexican Littoral Fundamental for Decision Making on Coastal Natural Resources. Available online: https://www.gob.mx/conabio/prensa/conabio-genera-nueva-cartografia-de-la-linea-de-costa-de-mexico?idiom=es (accessed on 26 November 2022).
4. Franco-Ochoa, C.; Zambrano-Medina, Y.; Plata-Rocha, W.; Monjardín-Armenta, S.; Rodríguez-Cueto, Y.; Escudero, M.; Mendoza, E. Long-Term Analysis of Wave Climate and Shoreline Change along the Gulf of California. *Appl. Sci.* **2020**, *10*, 8719. [CrossRef]
5. Piazza Forgiarini, A.P.; Amaral de Figueiredo, S.; Calliari, L.J.; Goulart, E.S.; Marques, W.; Trombetta, T.B.; Oleinik, P.H.; Guimarães, R.C.; Arigony-Neto, J.; Cabral Salame, C. Quantifying the Geomorphologic and Urbanization Influence on Coastal Retreat under Sea Level Rise. *Estuar. Coast. Shelf Sci.* **2019**, *230*, 106437. [CrossRef]
6. Özpolat, E.; Demir, T. The Spatiotemporal Shoreline Dynamics of a Delta under Natural and Anthropogenic Conditions from 1950 to 2018: A Dramatic Case from the Eastern Mediterranean. *Ocean Coast. Manag.* **2019**, *180*, 104910. [CrossRef]
7. Hamid, A.I.A.; Din, A.H.M.; Abdullah, N.M.; Yusof, N.; Hamid, M.R.A.; Shah, A.M. Exploring Space Geodetic Technology for Physical Coastal Vulnerability Index and Management Strategies: A Review. *Ocean Coast. Manag.* **2021**, *214*, 105916. [CrossRef]
8. Parthasarathy, K.S.S.; Deka, P.C. Remote Sensing and GIS Application in Assessment of Coastal Vulnerability and Shoreline Changes: A Review. *ISH J. Hydraul. Eng.* **2019**, *27*, 588–600. [CrossRef]
9. Roy, S.; Mahapatra, M.; Chakraborty, A. Shoreline Change Detection along the Coast of Odisha, India Using Digital Shoreline Analysis System. *Spat. Inf. Res.* **2018**, *26*, 563–571. [CrossRef]
10. Yan, D.; Yao, X.; Li, J.; Qi, L.; Luan, Z. Shoreline Change Detection and Forecast along the Yancheng Coast Using a Digital Shoreline Analysis System. *Wetlands* **2021**, *41*, 47. [CrossRef]
11. Williams, S.J. Sea-Level Rise Implications for Coastal Regions. *J. Coast. Res.* **2013**, *63*, 184–196. [CrossRef]
12. Chen, C.; Bu, J.; Zhang, Y.; Zhuang, Y.; Chu, Y.; Hu, J.; Guo, B. The Application of the Tasseled Cap Transformation and Feature Knowledge for the Extraction of Coastline Information from Remote Sensing Images. *Adv. Space Res.* **2019**, *64*, 1780–1791. [CrossRef]
13. Charles, W.F.; Makowski, C. *Encyclopedia of Coastal Science*; Springer: Berlin/Heidelberg, Germany, 2020. [CrossRef]
14. Daud, S.; Milow, P.; Rozainah; Zakaria, M. Analysis of Shoreline Change Trends and Adaptation of Selangor Coastline, Using Landsat Satellite Data. *J. Indian Soc. Remote Sens.* **2021**, *49*, 1869–1878. [CrossRef]
15. Zhang, Y.; Xie, J.; Liu, L. Investigating Sea-Level Change and Its Impact on Hong Kong's Coastal Environment. *Ann. GIS* **2011**, *17*, 105–112. [CrossRef]

16. Mujabar, P.S.; Chandrasekar, N. Shoreline Change Analysis along the Coast between Kanyakumari and Tuticorin of India Using Remote Sensing and GIS. *Arab. J. Geosci.* **2013**, *6*, 647–664. [CrossRef]

17. Appeaning Addo, K.; Jayson-Quashigah, P.N.; Kufogbe, K.S. Quantitative Analysis of Shoreline Change Using Medium Resolution Satellite Imagery in Keta, Ghana. *Mar. Sci.* **2012**, *1*, 1–9. [CrossRef]

18. Mutagi, S.; Yadav, A.; Hiremath, C.G. Shoreline Change Model: A Review. *Lect. Notes Civ. Eng.* **2022**, *162*, 1019–1031. [CrossRef]

19. Hossain, S.A.; Mondal, I.; Thakur, S.; Linh, N.T.T.; Anh, D.T. Assessing the Multi-Decadal Shoreline Dynamics along the Purba Medinipur-Balasore Coastal Stretch, India by Integrating Remote Sensing and Statistical Methods. *Acta Geophys.* **2022**, *70*, 1701–1715. [CrossRef]

20. Alesheikh, A.A.; Ghorbanali, A.; Nouri, N. Coastline Change Detection Using Remote Sensing. *Int. J. Environ. Sci. Technol.* **2007**, *4*, 61–66. [CrossRef]

21. Godwyn-Paulson, P.; Jonathan, M.P.; Roy, P.D.; Rodríguez-Espinosa, P.F.; Muthusankar, G.; Muñoz-Sevilla, N.P.; Lakshumanan, C. Evolution of Southern Mexican Pacific Coastline: Responses to Meteo-Oceanographic and Physiographic Conditions. *Reg. Stud. Mar. Sci.* **2021**, *47*, 101914. [CrossRef]

22. Williams, D.L.; Goward, S.; Arvidson, T. Landsat: Yesterday, Today, and Tomorrow. *Photogramm. Eng. Remote Sens.* **2006**, *72*, 1171–1178. [CrossRef]

23. Masria, A.; Nadaoka, K.; Negm, A.; Iskander, M. Detection of Shoreline and Land Cover Changes around Rosetta Promontory, Egypt, Based on Remote Sensing Analysis. *Land* **2015**, *4*, 216–230. [CrossRef]

24. Turner, I.L.; Harley, M.D.; Almar, R.; Bergsma, E.W.J. Satellite Optical Imagery in Coastal Engineering. *Coast. Eng.* **2021**, *167*, 103919. [CrossRef]

25. Randazzo, G.; Barreca, G.; Cascio, M.; Crupi, A.; Fontana, M.; Gregorio, F.; Lanza, S.; Muzirafuti, A. Analysis of Very High Spatial Resolution Images for Automatic Shoreline Extraction and Satellite-Derived Bathymetry Mapping. *Geosciences* **2020**, *10*, 172. [CrossRef]

26. Abdul Maulud, K.N.; Selamat, S.N.; Mohd, F.A.; Md Noor, N.; Wan Mohd Jaafar, W.S.; Kamarudin, M.K.A.; Ariffin, E.H.; Adnan, N.A.; Ahmad, A. Assessment of Shoreline Changes for the Selangor Coast, Malaysia, Using the Digital Shoreline Analysis System Technique. *Urban Sci.* **2022**, *6*, 71. [CrossRef]

27. Vallarino Castillo, R.; Negro Valdecantos, V.; Moreno Blasco, L. Shoreline Change Analysis Using Historical Multispectral Landsat Images of the Pacific Coast of Panama. *J. Mar. Sci. Eng.* **2022**, *10*, 1801. [CrossRef]

28. Himmelstoss, E.A.; Henderson, R.E.; Kratzmann, M.G.; Farris, A.S. *Digital Shoreline Analysis System (DSAS) Version 5.1 User Guide*; Open-File Report 2021-1091; USGS Publication Warehouse: Reston, VI, USA, 2021. [CrossRef]

29. Zambrano-medina, Y. Shoreline Analysis and Erosion Risk Assessment of a Coastal Strip Subjected to High Anthropogenic Pressure. *Tecnol. Cienc. Agua* **2022**, *13*, 249–300. [CrossRef]

30. Hakkou, M.; Maanan, M.; Belrhaba, T.; El khalidi, K.; El Ouai, D.; Benmohammadi, A. Multi-Decadal Assessment of Shoreline Changes Using Geospatial Tools and Automatic Computation in Kenitra Coast, Morocco. *Ocean Coast. Manag.* **2018**, *163*, 232–239. [CrossRef]

31. Dewidar, K.; Bayoumi, S. Forecasting Shoreline Changes along the Egyptian Nile Delta Coast Using Landsat Image Series and Geographic Information System. *Environ. Monit. Assess.* **2021**, *193*, 429. [CrossRef]

32. SEMARNAT Gulf of California: 1126 km of Imposing Beauty and Prodigal Biodiversity. Available online: https://www.gob.mx/ semarnat/articulos/golfo-de-california-mil-126-km-de-imponente-belleza-y-prodiga-biodiversidad-150945 (accessed on 15 August 2022).

33. Jiménez-Illescas, Á.R.; Zayas-Esquer, M.M.; Espinosa-Carreón, T.L. Integral Management of the Coastal Zone to Solve the Problems of Erosion in Las Glorias Beach, Guasave, Sinaloa, Mexico. In *Coastal Management*; Krishnamurthy, R.R., Jonathan, M.P., Srinivasalu, S., Glaeser, B., Eds.; Academic Press: Cambridge, MA, USA, 2019; pp. 141–163, ISBN 9780128104736.

34. Liu, D.; Xu, Y.; Faghihinia, M.; Kay, P.; Chan, F.K.S.; Wu, N. Evolving Framework of Studies on Global Gulf Ecosystems with Sustainable Development Goals. *Environ. Sci. Pollut. Res.* **2022**, *29*, 18385–18397. [CrossRef]

35. Vellanoweth, R.L.; Porcayo-Michelini, A.; Guttenberg, R.B.; Hayden, W.; Ainis, A.F.; Hernández-Estrada, R.L. Spring Tides, Storm Surges, and the Destruction of Coastal Middens: A Case Study from the Upper Gulf of California, México. *J. Isl. Coast. Archaeol.* **2020**, *17*, 420–431. [CrossRef]

36. Ledesma-Vázquez, J.; Johnson, M.E.; Gonzalez-Yajimovich, O.; Santamaría-del-Angel, E. Gulf of California Geography, Geological Origins, Oceanography, and Sedimentation Patterns. In *Atlas of Coastal Ecosystems in the Western Gulf of California*; The University of Arizona Press: Tucson, AZ, USA, 2009; pp. 1–10.

37. Nava-Sánchez, E.H.; Martínez-Flores, G.; Murillo-Jiménez, J.M. *Factors That Cause Beach Erosion in Baja California Sur, Mexico*; University of El Salvador: San Salvador, El Salvador, 2018; Volume 4.

38. Baig, M.R.I.; Ahmad, I.A.; Shahfahad; Tayyab, M.; Rahman, A. Analysis of Shoreline Changes in Vishakhapatnam Coastal Tract of Andhra Pradesh, India: An Application of Digital Shoreline Analysis System (DSAS). *Ann. GIS* **2020**, *26*, 361–376. [CrossRef]

39. Zed, A.A.A.; Soliman, M.R.; Yassin, A.A. Evaluation of Using Satellite Image in Detecting Long Term Shoreline Change along El-Arish Coastal Zone, Egypt. *Alex. Eng. J.* **2018**, *57*, 2687–2702. [CrossRef]

40. Sekovski, I.; Stecchi, F.; Mancini, F.; Del Rio, L. Image Classification Methods Applied to Shoreline Extraction on Very High-Resolution Multispectral Imagery. *Int. J. Remote Sens.* **2014**, *35*, 3556–3578. [CrossRef]

41. Tsai, Y.L.S. Monitoring 23-Year of Shoreline Changes of the Zengwun Estuary in Southern Taiwan Using Time-Series Landsat Data and Edge Detection Techniques. *Sci. Total Environ.* **2022**, *839*, 156310. [CrossRef] [PubMed]
42. Kankara, R.S.; Selvan, S.C.; Markose, V.J.; Rajan, B.; Arockiaraj, S. Estimation of Long and Short Term Shoreline Changes along Andhra Pradesh Coast Using Remote Sensing and GIS Techniques. *Procedia Eng.* **2015**, *116*, 855–862. [CrossRef]
43. Jalaludin, M.; Setiawan, C.; Zid, M.; Utomo, R.T. Analysis of Shoreline Changes before and after the Tsunami at Tanjung Lesung Beach, Banten Province of Indonesia. *IOP Conf. Ser. Earth Environ. Sci.* **2020**, *412*, 012004. [CrossRef]
44. Kermani, S.; Boutiba, M.; Guendouz, M.; Guettouche, M.S.; Khelfani, D. Detection and Analysis of Shoreline Changes Using Geospatial Tools and Automatic Computation: Case of Jijelian Sandy Coast (East Algeria). *Ocean Coast. Manag.* **2016**, *132*, 46–58. [CrossRef]
45. Barbaro, G.; Bombino, G.; Foti, G.; Borrello, M.M.; Puntorieri, P. Shoreline Evolution near River Mouth: Case Study of Petrace River (Calabria, Italy). *Reg. Stud. Mar. Sci.* **2019**, *29*, 100619. [CrossRef]
46. McFeeters, S.K. The Use of the Normalized Difference Water Index (NDWI) in the Delineation of Open Water Features. *Int. J. Remote Sens.* **1996**, *17*, 1425–1432. [CrossRef]
47. Mondejar, J.P.; Tongco, A.F. Near Infrared Band of Landsat 8 as Water Index: A Case Study around Cordova and Lapu-Lapu City, Cebu, Philippines. *Sustain. Environ. Res.* **2019**, *29*, 16. [CrossRef]
48. Ashtekar, A.S.; Mohammed-Aslam, M.A.; Moosvi, A.R. Utility of Normalized Difference Water Index and GIS for Mapping Surface Water Dynamics in Sub-Upper Krishna Basin. *J. Indian Soc. Remote Sens.* **2019**, *47*, 1431–1442. [CrossRef]
49. Liu, Y.; Wang, X.; Ling, F.; Xu, S.; Wang, C. Analysis of Coastline Extraction from Landsat-8 OLI Imagery. *Water* **2017**, *9*, 816. [CrossRef]
50. Crowell, M.; Leatherman, S.P.; Buckley, M.K. Historical Shoreline Change: Error Analysis and Mapping Accuracy. *J. Coast. Res.* **1991**, *7*, 839–852.
51. Kumar Das, S.; Sajan, B.; Ojha, C.; Soren, S. Shoreline Change Behavior Study of Jambudwip Island of Indian Sundarban Using DSAS Model. *Egypt. J. Remote Sens. Space Sci.* **2021**, *24*, 961–970. [CrossRef]
52. Kuleli, T.; Guneroglu, A.; Karsli, F.; Dihkan, M. Automatic Detection of Shoreline Change on Coastal Ramsar Wetlands of Turkey. *Ocean Eng.* **2011**, *38*, 1141–1149. [CrossRef]
53. Douglas, B.C.; Crowell, M. Long-Term Shoreline Position Prediction and Error Propagation. *J. Coast. Res.* **2000**, *16*, 145–152.
54. Genz, A.S.; Fletcher, C.H.; Dunn, R.A.; Frazer, L.N.; Rooney, J.J. The Predictive Accuracy of Shoreline Change Rate Methods and Alongshore Beach Variation on Maui, Hawaii. *J. Coast. Res.* **2007**, *23*, 87–105. [CrossRef]
55. Coca, O.; Ricaurte-Villota, C. Regional Patterns of Coastal Erosion and Sedimentation Derived from Spatial Autocorrelation Analysis: Pacific and Colombian Caribbean. *Coasts* **2022**, *2*, 125–151. [CrossRef]
56. Dar, I.A.; Dar, M.A. Prediction of Shoreline Recession Using Geospatial Technology: A Case Study of Chennai Coast, Tamil Nadu, India. *J. Coast. Res.* **2009**, *25*, 1276–1286. [CrossRef]
57. Vu, M.T.; Lacroix, Y.; Than, V.V.; Nguyen, V.T. Prediction of Shoreline Changes in Almanarre Beach Using Geospatial Techniques. *Indian J. Geo Mar. Sci.* **2020**, *49*, 207–2017.
58. Kalman, R.E. A New Approach to Linear Filtering and Prediction Problems. *J. Basic Eng.* **1960**, *82*, 35–45. [CrossRef]
59. Long, J.W.; Plant, N.G. Extended Kalman Filter Framework for Fore-Casting Shoreline Evolution. *Geophys. Res. Lett.* **2012**, *39*, 13603. [CrossRef]
60. Molina, R.; Anfuso, G.; Manno, G.; Prieto, F.J.G. The Mediterranean Coast of Andalusia (Spain): Medium-Term Evolution and Impacts of Coastal Structures. *Sustainability* **2019**, *11*, 3539. [CrossRef]
61. Jiménez-Illescas, A.R.; Ma Magdalena, Z.E.; Leticia, E.C.T. Integral Management of the Coastal Zone to Solve the Problems of Erosion in Las Glorias Beach, Guasave, Sinaloa, Mexico. *Coast. Manag. Glob. Chall. Innov.* **2018**, 141–163. [CrossRef]
62. Laksono, F.A.T.; Borzì, L.; Distefano, S.; Di Stefano, A.; Kovács, J. Shoreline Prediction Modelling as a Base Tool for Coastal Management: The Catania Plain Case Study (Italy). *J. Mar. Sci. Eng.* **2022**, *10*, 1988. [CrossRef]
63. Oyedotun, T.D.T.; Ruiz-Luna, A.; Navarro-Hernández, A.G. Contemporary Shoreline Changes and Consequences at a Tropical Coastal Domain. *Geol. Ecol. Landsc.* **2018**, *2*, 104–114. [CrossRef]
64. Montaño-Ley, Y.; Carbajal, N.; Páez-Osuna, F. Bed Load Transport of Sediments and Morphodynamics in the Topolobampo Coastal Lagoon System, Mexico. *J. Coast. Conserv.* **2014**, *18*, 55–67. [CrossRef]
65. Hernández Azcúnaga, L. *Sediment Transport Dynamics as Bottom Load in the Upper Gulf of California*; Potosino Institute of Scientific and Technological Research: San Luis, Mexico, 2005.
66. Carriquiry, J.D.; Sánchez, A. Sedimentation in the Colorado River Delta and Upper Gulf of California after Nearly a Century of Discharge Loss. *Mar. Geol.* **1999**, *158*, 125–145. [CrossRef]
67. Carriquiry, J.D.; Sánchez, A.; Camacho-Ibar, V.F. Sedimentation in the Northern Gulf of California after Cessation of the Colorado River Discharge. *Sediment. Geol.* **2001**, *144*, 37–62. [CrossRef]
68. Lizarraga, O. Impacts of US Residential Tourism in Northwest Mexican Coastal Destinations: The Cases of Mazatlán, Sinaloa; Cabo San Lucas, Baja California Sur and Puerto Peñasco, Sonora. *Rev. Lat.-Am. Tur.* **2019**, *5*, 1–14. [CrossRef]
69. Lluch-Cota, S.E.; Aragón-Noriega, E.A.; Arreguín-Sánchez, F.; Aurioles-Gamboa, D.; Jesús Bautista-Romero, J.; Brusca, R.C.; Cervantes-Duarte, R.; Cortés-Altamirano, R.; Del-Monte-Luna, P.; Esquivel-Herrera, A.; et al. The Gulf of California: Review of Ecosystem Status and Sustainability Challenges. *Prog. Oceanogr.* **2007**, *73*, 1–26. [CrossRef]

70. Castillo, M.; Muñoz-Salinas, E.; Sanderson, D.C.W.; Cresswell, A. Landscape Evolution of Punta Arena Sand Spit (SE Baja California Peninsula, NW Mexico): Implications of ENSO on Landscape Erosion Rates. *Catena* **2020**, *193*, 104601. [CrossRef]
71. Johnson, M.E.; Johnson, E.M.; Guardado-France, R.; Ledesma-Vázquez, J. Holocene Hurricane Deposits Eroded as Coastal Barriers from Andesite Sea Cliffs at Puerto Escondido (Baja California Sur, Mexico). *J. Mar. Sci. Eng.* **2020**, *8*, 75. [CrossRef]